Materials Research Proceedings **4** (2018) 17-22 doi: http://dx.doi.org/10.21741/9781945291678-3

In situ Synchrotron X-ray Measurement of Strain Fields near Fatigue Cracks grown in Hydrogen

M. Connolly[1,a*], P. Bradley[1,b], A. Slifka[1,c], D. Lauria[1,d] and E. Drexler[1,e]

[1]National Institute of Standards and Technology, 325 Broadway Boulder, CO 80305 USA

[a]matthew.connolly@nist.gov, [b]peter.bradley@nist.gov, [c]andrew.slifka@nist.gov, [d]damian.lauria@nist.gov, [e]elizabeth.drexler@nist.gov

Keywords: Strain, Hydrogen, Fracture, Fatigue, Synchrotron, Diffraction

Abstract. The embrittlement and enhanced fatigue crack growth rate of metals in the presence of hydrogen is a long-standing problem [1-5]. In an effort to determine the dominant damage mechanism behind hydrogen-assisted fatigue crack growth, we performed high-energy X-ray diffraction (HEXRD) measurements to characterize the strain fields near cracks grown both in air, as well as in a hydrogen environment. An enhancement in the magnitude and spatial extent of the strain field near the crack grown in hydrogen compared with the strain field near the crack grown in air was observed. We discuss the differences between the measured in-air and in-hydrogen crack-tip strain fields in the context of the two leading damage mechanisms proposed in the literature.

Introduction

Proposed mechanisms of hydrogen embrittlement include hydrogen-enhanced decohesion (HEDE) and the hydrogen-enhanced localized plasticity (HELP) [6-10]. In the HEDE mechanism, decohesion occurs either through a weakening of Fe-Fe bonds ("intra-lattice" decohesion) or from a buildup of hydrogen at grain boundaries ("inter-lattice decohesion"). In the HELP mechanism, the introduction of hydrogen gas leads to failure through localized plastic deformation from enhancement of dislocation mobility in the steel framework. Quantifying strain fields from fatigue cracking is crucial to the understanding of the underlying mechanism(s) behind hydrogen embrittlement (HE) and to the study of HE and hydrogen-assisted fatigue crack growth rate (HA-FCGR). For example, a measurement of the strain field ahead of a crack tip can directly confirm predictions from the HEDE mechanism of intra-lattice decohesion.

The synchrotron source available at Argonne National Laboratory's Advanced Photon Source (APS) and its HEXRD technique on the 1-ID beamline are useful tools for probing the strain field ahead of cracks grown in hydrogen. The use of a 2D detector and short X-ray wavelengths allows for the simultaneous measurement of the two in-plane strain components in the planar, compact tension (C(T)) specimen geometry commony used for FCGR measurements. The load frame available at APS for mechanical testing is capable of fatigue cycling up to 10 Hz, which allows a full FCGR test to be performed within a single awarded beam time. Further, high energy X-rays have high flux and high penetration through sample chamber materials, which allow for *in situ* measurements. For HE and HA-FCGR studies, *in situ* measurements are crucial because of the rapid diffusion of hydrogen out of ferritic steels. Even after extended exposure to hydrogen, the deleterious effect of hydrogen on ferritic steels after the specimen has been removed from the hydrogen environment for just a short period of time (~ 15 min) [7]. Therefore, in order to fully understand the HA-FCGR mechanism, it is necessary to perform any measurements *in situ*.

Materials Research Proceedings **4** (2018) 17-22 doi: http://dx.doi.org/10.21741/9781945291678-3

Materials

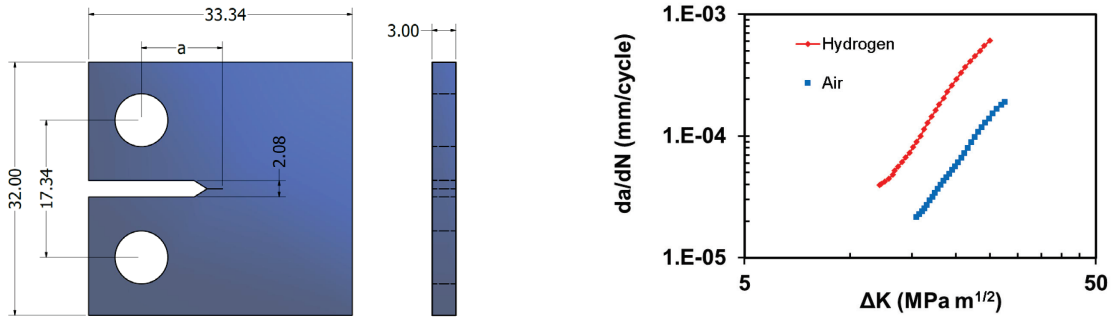

Fig. 1: Geometry of the X100 steel CT specimen used for HEXRD measurements (left). Units are in mm. FCGR curves for the 4130 steel showing a significant enhancement in FCGR in hydrogen compared to in air (right).

The material used for this study was a 4130 steel in a compact tension (CT) geometry, with dimensions as shown in Fig. 1 (left). These type of quench and temper steels exhibit a drastic increase in FCGR for fatigue cracks grown in hydrogen compared to those grown in air (Fig. 1, right).

Experimental Methods

The X-ray measurements were performed with a chamber designed for use in neutron and X-ray scattering measurements of metallic specimens under mechanical load in up to 1.7 MPa gaseous atmosphere [11]. At beamline 1-ID [12, 13], X-rays produced by the synchrotron source are monochromated with a bent Si(111) crystal. The beam is then narrowed by the beam slit, which results in a minimum beam size of 20 μm × 20 μm. For experiments that use the hydrogen chamber, the chamber is mounted to the mechanical load frame, and the load frame is mounted on a stage capable of translations perpendicular to the beam in the horizontal and vertical directions. Five helium purges and five hydrogen purges were performed at pressures of 1.7 MPa to clean the chamber prior to fatigue testing. Commerical purity helium (99.995 % pure) and research-grade hydrogen (99.9995 %) were used. The pressure was maintined at 1.7 MPa throughout the course of the X-ray measurements.

The X-ray measurements were performed with 80.725 keV (λ = 0.15359 Å) X-rays. The X-ray beam size was 20 μm × 20 μm, which determines the spatial resolution of the strain mapping. For the diffraction measurements, a pixelated area detector with a pixel pitch of 200 μm and 2048 × 2048 pixel array was used. Radiographs were collected with a camera that has an effective pixel size of 1 μm after lensing. The radiograph detector was positioned between the sample and diffraction detector during radiograph measurements, and was moved out of the beam by a translation stage for diffraction measurements. The mechanical load frame was a modified servo-hydraulic system with a force capacity of +/- 15 kN and was equipped with a 2.5 kN load cell, mounted above the chamber. A 44 kN load cell was mounted inside the sample chamber at the base of the load train. A crack mouth opening displacement (CMOD) gauge was attached to the CT specimen at the load line. Fatigue cycling was performed in displacement control with a frequency of 1 Hz. To determine the unstrained lattice spacing, the lattice spacing was measured on an illuminated spot far from the crack tip when the specimen was under zero load. By using as a reference parameter the lattice spacing far from the crack tip while the material was in air, the reported strain measurements then incorporate both the effect of interstitial hydrogen [14] as well as the response of the applied stress, to describe the full deformation at the crack tip. In the unloaded specimen, the variance in the lattice spacing

Materials Research Proceedings **4** (2018) 17-22 doi: http://dx.doi.org/10.21741/9781945291678-3

throughout the scanned material was on the order of 10^{-4}, leading to a systematic uncertainty in the strain of 50 μstrain.

Results and Discussion

Crack tip radiographs. Radiographs of the crack grown in hydrogen, after N = 20,000 cycles, N = 38,000 cycles, and N = 54,000 cycles, and in air after N = 0, N = 100,000, and N = 149,000 cycles with a load of 1700 N applied are shown in Fig. 2.

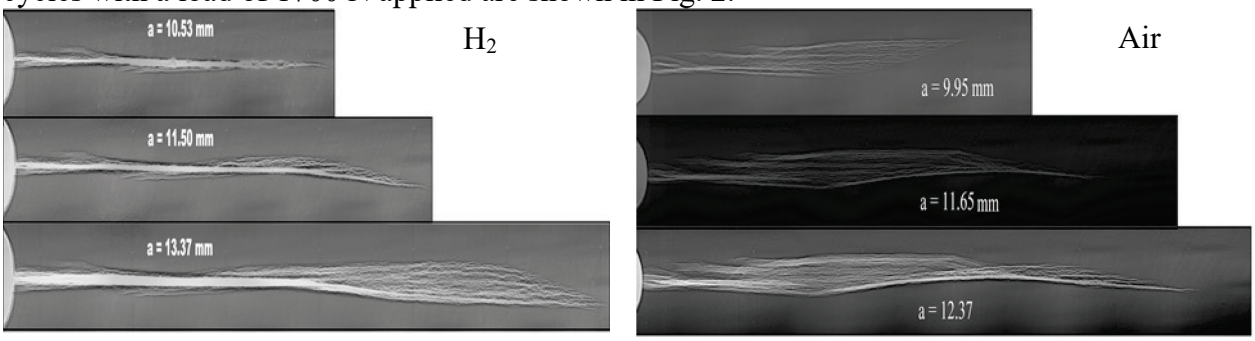

Fig. 2: X-ray radiographs of the crack tip with an applied force of 1700 N after N = 20,000 cycles, N = 38,000 cycles, and N = 54,000 cycles grown in hydrogen, and for N = 0 cycles, N = 100,000 cycles, and N = 149,000 cycles in air (from top to bottom).

For the crack grown in H_2 the crack lengths shown in Fig. 2 (left) correspond to ΔK = 12.28 MPa $\sqrt{m}$, ΔK = 13.54 MPa $\sqrt{m}$, and ΔK = 16.58 MPa $\sqrt{m}$, which reside at the start, middle, and end of the "knee" in the hydrogen da/dN curve shown in Fig. 1. Likewise, the air cracks shown in Fig. 2 (right) correspond to ΔK = 11.7 MPa $\sqrt{m}$, ΔK = 13.7 MPa $\sqrt{m}$, and ΔK = 14.9 MPa $\sqrt{m}$. The 2D radiographs are a projection of the 3D attenuation coefficient summed through the thickness of the specimen. The multiple crack branches observed in each image therefore correspond to the crack growing in different planes. Similar crack branching has been observed using synchrotron radiography in a fretting crack grown in a 2024 aluminum alloy [15]. In the first two images of the crack grown in hydrogen, some crack branching is observed behind the tip of the crack, however the crack tip is much sharper than the final hydrogen crack image or any of the air crack images. It is interesting to note the crack grown in air exhibits far greater crack branching when the crack is short, whereas the hydrogen crack does not exhibit secondary damage to the same extent until the crack is longer (corresponding to higher ΔK).

Fig. 3 shows the loading direction strain (ε_{yy}) as a function of distance ahead of the crack tip, *r,* for the six crack conditions shown in Fig. 2. Closest to the crack, the expected $r^{-1/2}$ strain dependence is observed until ~ 3 mm ahead of the crack tip. Far from the crack tip in the longest cracks, compressive strain is observed attributable to hinging of the CT specimen. In the shorter cracks (< 11 mm) the strain field forms a sharp cusp at r = 0. In the longer cracks with P = 850 N, the strain magnitude increases moving away from the crack tip, until it reaches a maximum at ~ 0.25 mm, then decreases with $r^{-1/2}$ dependence. The lowered elastic strain nearest the crack tip is likely from the build up of plastic deformation during fatigue cycling. The magnitude of the drop in strain at the crack tip is significantly higher in the crack grown in hydrogen compared with that of the crack grown in air (400 μstrain compared with 100 μstrain). This may suggest additional plastic deformation localized at the crack tip from the presence of hydrogen. Enhanced near-crack plastic deformation is consistent with the HELP mechanism. The extent of the plastic deformation can be quantified in the dislocation density that is determined through peak broadening analysis; however, the current work focuses on the elastic strain only.

Materials Research Proceedings **4** (2018) 17-22 doi: http://dx.doi.org/10.21741/9781945291678-3

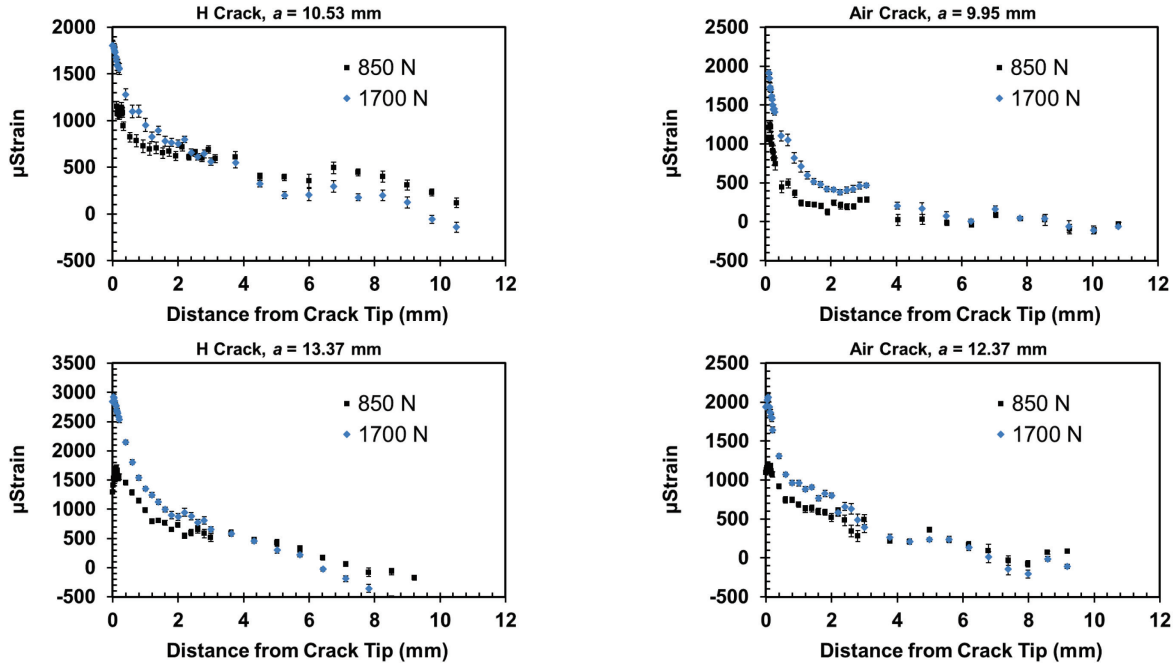

Fig. 3: Loading direction (ε_{yy}) strain values near cracks grown in hydrogen (left) and in air (right), with 1700 N and 850 N of applied load.

In comparing the hydrogen and air cracks, both the maximum strain magnitude is enhanced for the crack grown in hydrogen compared with that grown in air. The rate at which the strain drops as a function of distance from the crack is lower for the crack grown in hydrogen. These differences are shown most predominately in Fig. 4, which shows the crack-tip strain values in the loading direction ahead of cracks grown in air compared with one grown in hydrogen with the same crack length of a = 11.5 mm. The largest difference between the two strain fields are for r < 2 mm ahead of the crack tip. The crack strain field in air decays very sharply to within 25 % of its maximum by r = 2 mm ahead of the crack tip, whereas the decay of the crack strain field in hydogen is much shallower, reaching 25 % of its maximum near r = 3 mm. Beyond this region, the strain fields are nearly independent of applied load.

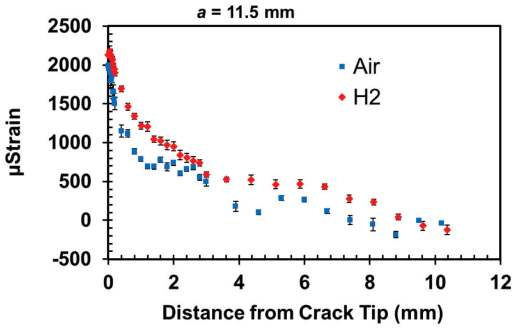

Fig. 4: Strain fields (ε_{yy}) corresponding to the loading direction near cracks grown in hydrogen and air for an 11.5 mm crack.

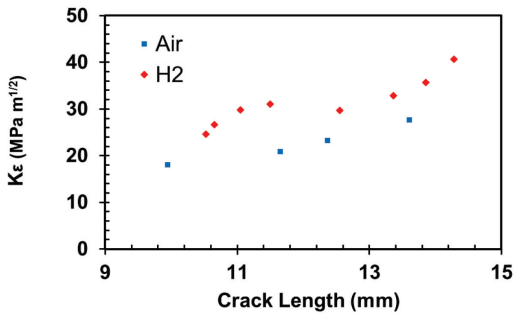

Fig. 5: Strain-based crack tip deformation parameter K_ε as a function of crack length for cracks grown in air and in hydrogen.

Although the strain fields were measured under static loads, we can relate the differences in static crack-tip strain fields to measured FCGR. For r within the "K-dominant region"[16] (that

Materials Research Proceedings **4** (2018) 17-22 doi: http://dx.doi.org/10.21741/9781945291678-3

is, for r greater than the size of the plastic zone but sufficiently far from the specimen edge to avoid significant influence from the specimen boundary), the K parameter completely defines the strain field ahead of the crack tip. Visual inspection of the measured strain fields indicates the K-dominant region to be approximately 0.5 mm < r < 3 mm. Based on the strain fields measured here, the use of the ΔK prescribed by ASTM E647 [17], the standard test method for measuring FCGRs, does not accurately describe either the in-air and in-hydrogen fatigue cracks. Therefore the independent variable in the FCGR curves must be modified in order to correctly normalize the data with respect to the true deformation state at the crack tip. These data suggests the correct normalization should be done with respect to the strain rather than the applied stress state as in the ΔK formulation in ASTM E-647. Here we define a new parameter K_ε which satisfies

$$\sigma_{ij}(r,\theta) = \frac{K_\varepsilon}{\sqrt{2\pi r}} f_{ij}(\theta), \tag{1}$$

where r and θ are the distance from the crack tip and angle with respect to the crack, respectively, and $f_{ij}(\theta)$ is a geometrical factor. Assuming plane-stress conditions the loading-direction strain, ϵ_{yy}, is

$$\epsilon_{yy} = \frac{1}{E}(-\nu\,\sigma_{xx} + \sigma_{yy}), \tag{2}$$

where ν is Poisson's ratio and E is Young's modulus. With $\theta = 0$, substituting Eq. (1) into (2) gives:

$$\epsilon_{yy} = \frac{(1-\nu)}{E}\left(\frac{K_\varepsilon}{\sqrt{2\pi r}}\right). \tag{3}$$

With Eq. (3), we fit the measured strain fields ϵ_{yy} at $\theta = 0$ to determine the strain-based K_ε parameter for each environmental condition and crack length. Fig. 5 shows K_ε as a function of crack length for the cracks grown in air and in hydrogen with an applied load of P = 1700 N. For each crack extension, K_ε for the crack grown in hydrogen is larger than that for the crack grown in air by ~ 50 %.

Conclusion

We have shown through *in situ* HEXRD strain mapping an enhancement in the magnitude of the crack-tip strain attributable to the presence of hydrogen. The results presented here are consistent with the intra-lattice HEDE mechanism. The enhancement suggests that a strain-based parameter is better suited for hydrogen FCGR measurements in order to accurately describe the crack-tip deformation state and for comparing air and hydrogen FCGRs. For the 4130 steel and crack lengths measured here, we observe a ~50 % enhancement of the strain-based parameter in hydrogen compared with that in air. Radiographs of the crack tip show significant differences between air and hydrogen cracks.

References

[1] J.R. Fekete, J.W. Sowards and R.L. Amaro, Economic impact of applying high strength steels in hydrogen gas pipelines, Int. J. Hydrog. Energy. 40(33) (2015) 10547-10558. https://doi.org/10.1016/j.ijhydene.2015.06.090

[2] W.C. Leighty, J. Holloway, R. Merer, G. Keith and D.E. White, Compressorless hydrogen transmission pipelines deliver large-scale stranded renewable energy at competitive cost, Proceedings of the 23rd World Gas Conference (2006)

[3] A.J. Slifka, E.S. Drexler, N.E.Nanninga, Y.S. Levy, J.D. McColskey, R.L. Amaro and A.E. Stevenson, Fatigue crack growth of two pipeline steels in a pressurized hydrogen environment, Corros. Sci. 78 (2014) 313-321. https://doi.org/10.1016/j.corsci.2013.10.014

[4] N.E. Nanninga, Y.S. Levy, E.S. Drexler, R.T. Condon, A.E. Stevenson and A.J. Slifka, Comparison of hydrogen embrittlement in three pipeline steels in high pressure gaseous hydrogen environments, Corros. Sci. 59 (2012) 1-9. https://doi.org/10.1016/j.corsci.2012.01.028

[5] R.L. Amaro, N. Rustagi, K.O. Findley, E.S. Drexler and A.J. Slifka, Modeling the fatigue crack growth of X100 pipeline steel in gaseous hydrogen, Int. J. Fatigue. 59 (2014) 262-271. https://doi.org/10.1016/j.ijfatigue.2013.08.010

[6] R.A. Oriani, A mechanistic theory of hydrogen embrittlement of steels, Berichte der Bunsengesellschaft für physikalische Chemie 76(8) (1972) 848-857.

[7] P.P. Darcis, J.D. McColskey, A.N. Lasseigne and T.A. Siewert, Hydrogen effects on fatigue crack growth rate in high strength pipeline steel, Effects of Hydrogen on Materials: Proceedings of the 2008 International Hydrogen Conference (2009) 381.

[8] T. Tabata and H.K Birnbaum, Direct observations of the effect of hydrogen on the behavior of dislocations in iron, Scr. Metall. 17(7) (1983) 947-950. https://doi.org/10.1016/0036-9748(83)90268-5

[9] H.K. Birnbaum and P. Sofronis Hydrogen-enhanced localized plasticity—a mechanism for hydrogen-related fracture, Mater. Sci. Eng. A 176(1-2) (1994) 191-202. https://doi.org/10.1016/0921-5093(94)90975-X

[10] I.M. Robertson, P. Sofronis, A. Nagao, M.L. Martin, S. Wang, D.W. Gross and K.E. Nygren, Hydrogen embrittlement understood, Metall. Mater. Trans. A 46(6) (2015) 2323-2341. https://doi.org/10.1007/s11661-015-2836-1

[11] M.J. Connolly, P.E. Bradley, A.J. Slifka and E.S. Drexler, Chamber for mechanical testing in H2 with observation by neutron scattering, Rev. Sci. Instrum. 88(6) (2017) 063901. https://doi.org/10.1063/1.4986471

[12] J. Almer, Advanced Photon Source. Retrieved July 20, 2017, from https://www1.aps.anl.gov/sector-1/1-id

[13] A.S. Gill, Z. Zhou, U. Lienert, J. Almer, D.F Lahrman, S.R. Mannava and V.K. Vasudevan, High spatial resolution, high energy synchrotron X-ray diffraction characterization of residual strains and stresses in laser shock peened Inconel 718SPF alloy, J. Appl. Phys. 111(8) (2012) 084904. https://doi.org/10.1063/1.3702890

[14] G.L. Nash, H. Choo, P. Nash, L.L. Daemen and A.M. Bourke, Lattice Dilation in a Hydrogen Charged Steel, International Centre for Diffraction Data. Adv. X-Ray Anal. (2003) 238-239.

[15] H. Proudhon, J.Y. Buffière and S. Fouvry, Three-dimensional study of a fretting crack using synchrotron X-ray micro-tomography, Eng. Fract. Mech. 74(5) (2007) 782-793. https://doi.org/10.1016/j.engfracmech.2006.06.019

[16] Anderson, T. L. (2017). Fracture mechanics: fundamentals and applications, second ed., CRC press, Boca Raton, 1995.

[17] ASTM International, Standard test method for measurement of fatigue crack growth rates. (2011)